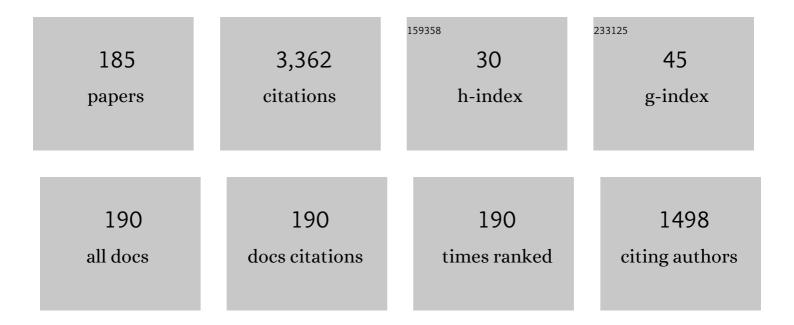
List of Publications by Year in descending order

Source: https://exaly.com/author-pdf/6091648/publications.pdf Version: 2024-02-01



YINRIN YAO

#	Article	IF	CITATIONS
1	Hourly Rainfall Forecast Model Using Supervised Learning Algorithm. IEEE Transactions on Geoscience and Remote Sensing, 2022, 60, 1-9.	2.7	31
2	Near Real-Time Global Ionospheric Modeling Based on an Adaptive Kalman Filter State Error Covariance Matrix Determination Method. IEEE Transactions on Geoscience and Remote Sensing, 2022, 60, 1-12.	2.7	4
3	Adaptive AOD Forecast Model Based on GNSS-Derived PWV and Meteorological Parameters. IEEE Transactions on Geoscience and Remote Sensing, 2022, 60, 1-10.	2.7	4
4	Two-Step Precipitable Water Vapor Fusion Method. IEEE Transactions on Geoscience and Remote Sensing, 2022, 60, 1-10.	2.7	8
5	Conventional and neural network-based water vapor density model for GNSS troposphere tomography. GPS Solutions, 2022, 26, 1.	2.2	7
6	FY-3A/MERSI precipitable water vapor reconstruction and calibration using multi-source observation data based on a generalized regression neural network. Atmospheric Research, 2022, 265, 105893.	1.8	11
7	Adaptive Aerosol Optical Depth Forecasting Model Using GNSS Observation. IEEE Transactions on Geoscience and Remote Sensing, 2022, 60, 1-9.	2.7	6
8	Improving the accuracy and spatial resolution of precipitable water vapor dataset using a neural network-based downscaling method. Atmospheric Environment, 2022, 269, 118850.	1.9	6
9	Quantitatively Analyzing the Impacts of Seasonal Water Storage Changes in the Three Gorges Reservoir on Nearby Crust. Pure and Applied Geophysics, 2022, 179, 817.	0.8	1
10	Reconstructing the data gap between GRACE and GRACE follow-on at the basin scale using artificial neural network. Science of the Total Environment, 2022, 823, 153770.	3.9	11
11	Daytime F Region Echoes at Equatorial Ionization Anomaly Crest During Geomagnetic Quiet Period: Observations From Multiâ€Instruments. Space Weather, 2022, 20, .	1.3	2
12	Research on the ionospheric diurnal Double-Maxima patterns in Asia-Australian area based on the VTEC observations of BDS geostationary satellites. Advances in Space Research, 2022, , .	1.2	1
13	Threeâ€Dimensional Reconstruction of Tongue of Ionization During the 11 October 2010 Geomagnetic Storm and Evolution Analysis With TIEGCM. Space Weather, 2022, 20, .	1.3	1
14	Bridging the data gap between GRACE and GRACE-FO using artificial neural network in Greenland. Journal of Hydrology, 2022, 608, 127614.	2.3	9
15	Editing arcs to improve the capacity of GNSS-IR for soil moisture retrieval in undulating terrains. GPS Solutions, 2022, 26, 1.	2.2	14
16	An Improved MODIS NIR PWV Retrieval Algorithm Based on an Artificial Neural Network Considering the Land-Cover Types. IEEE Transactions on Geoscience and Remote Sensing, 2022, 60, 1-12.	2.7	9
17	A novel ionospheric mapping function modeling at regional scale using empirical orthogonal functions and GNSS data. Journal of Geodesy, 2022, 96, 1.	1.6	5
18	Precipitable water vapor fusion method based on artificial neural network. Advances in Space Research, 2022, 70, 85-95.	1.2	6

#	Article	IF	CITATIONS
19	Jointly using the GLDAS 2.2 model and GRACE to study the severe Yangtze flooding of 2020. Journal of Hydrology, 2022, 610, 127927.	2.3	8
20	GNSS-derived PWV and meteorological data for short-term rainfall forecast based on support vector machine. Advances in Space Research, 2022, 70, 992-1003.	1.2	2
21	Retrieval of high spatial resolution precipitable water vapor maps using heterogeneous earth observation data. Remote Sensing of Environment, 2022, 278, 113100.	4.6	16
22	Analysis of the 3-D Evolution Characteristics of Ionospheric Anomalies During a Geomagnetic Storm Through Fusion of GNSS and COSMIC-2 Data. IEEE Transactions on Geoscience and Remote Sensing, 2022, 60, 1-19.	2.7	2
23	Transformer-Based Global Zenith Tropospheric Delay Forecasting Model. Remote Sensing, 2022, 14, 3335.	1.8	4
24	An Updated Experimental Model of IGâ,â,, Indices Over the Antarctic Region via the Assimilation of IRI2016 With GNSS TEC. IEEE Transactions on Geoscience and Remote Sensing, 2021, 59, 1700-1717.	2.7	7
25	An Improved Computerized Ionospheric Tomography Model Fusing 3-D Multisource Ionospheric Data Enabled Quantifying the Evolution of Magnetic Storm. IEEE Transactions on Geoscience and Remote Sensing, 2021, 59, 3725-3736.	2.7	3
26	A new three-dimensional computerized ionospheric tomography model based on a neural network. GPS Solutions, 2021, 25, 1.	2.2	20
27	GNSS-Based Statistical Analysis of Ionospheric Anomalies During Typhoon Landings in Taiwan/Japan. IEEE Transactions on Geoscience and Remote Sensing, 2021, 59, 5272-5279.	2.7	4
28	Retrieval of a High-Precision Drought Monitoring Index by Using GNSS-Derived ZTD and Temperature. IEEE Journal of Selected Topics in Applied Earth Observations and Remote Sensing, 2021, 14, 8730-8743.	2.3	6
29	Accuracy Analysis of International Reference Ionosphere 2016 and NeQuick2 in the Antarctic. Sensors, 2021, 21, 1551.	2.1	6
30	Precipitable water vapor fusion based on a generalized regression neural network. Journal of Geodesy, 2021, 95, 1.	1.6	39
31	Study of Spatial and Temporal Variations of Ionospheric Total Electron Content in Japan, during 2014–2019 and the 2016 Kumamoto Earthquake. Sensors, 2021, 21, 2156.	2.1	3
32	Improving the Estimation of Weighted Mean Temperature in China Using Machine Learning Methods. Remote Sensing, 2021, 13, 1016.	1.8	26
33	Interannual ice mass variations over the Antarctic ice sheet from 2003 to 2017 were linked to El Niño-Southern Oscillation. Earth and Planetary Science Letters, 2021, 560, 116796.	1.8	14
34	High temporal resolution global PWV dataset of 2005–2016 by using a neural network approach to determine the mean temperature of the atmosphere. Advances in Space Research, 2021, 67, 3087-3097.	1.2	9
35	Recent trends in precipitation over the Myanmar Coast during onset and withdrawal phases of monsoon season. Theoretical and Applied Climatology, 2021, 145, 363-376.	1.3	4
36	Regional GNSS-Derived SPCI: Verification and Improvement in Yunnan, China. Remote Sensing, 2021, 13, 1918.	1.8	10

#	Article	IF	CITATIONS
37	Three-dimensional reconstruction of seismo-traveling ionospheric disturbances after March 11, 2011, Japan Tohoku earthquake. Journal of Geodesy, 2021, 95, 1.	1.6	5
38	An Improved Single-Epoch Attitude Determination Method for Low-Cost Single-Frequency GNSS Receivers. Remote Sensing, 2021, 13, 2746.	1.8	3
39	Characterization of Highâ€m ULF Wave Signatures in GPS TEC Data. Geophysical Research Letters, 2021, 48, e2021GL094282.	1.5	6
40	A Regional Model for Predicting Tropospheric Delay and Weighted Mean Temperature in China Based on GRAPES_MESO Forecasting Products. Remote Sensing, 2021, 13, 2644.	1.8	8
41	A novel method of retrieving potential ET in China. Journal of Hydrology, 2021, 598, 126271.	2.3	11
42	Ordered Subsets-Constrained ART Algorithm for Ionospheric Tomography by Combining VTEC Data. IEEE Transactions on Geoscience and Remote Sensing, 2021, 59, 7051-7061.	2.7	9
43	GRACE and land surface models reveal severe drought in eastern China in 2019. Journal of Hydrology, 2021, 601, 126640.	2.3	20
44	A novel ENSO monitoring index and its potential for drought application. Journal of Atmospheric and Solar-Terrestrial Physics, 2021, 225, 105762.	0.6	5
45	A global empirical orthogonal function model of plasmaspheric electron content. Advances in Space Research, 2020, 65, 138-151.	1.2	2
46	Hourly PWV Dataset Derived from GNSS Observations in China. Sensors, 2020, 20, 231.	2.1	25
47	Multi-scale ionosphere responses to the May 2017 magnetic storm over the Asian sector. GPS Solutions, 2020, 24, 1.	2.2	14
48	Improving the estimate of the secular variation of Greenland ice mass in the recent decades by incorporating a stochastic process. Earth and Planetary Science Letters, 2020, 549, 116518.	1.8	12
49	A Refined Tomographic Window for GNSS-Derived Water Vapor Tomography. Remote Sensing, 2020, 12, 2999.	1.8	4
50	Forecasting Global Ionospheric TEC Using Deep Learning Approach. Space Weather, 2020, 18, e2020SW002501.	1.3	80
51	A New GNSS-Derived Water Vapor Tomography Method Based on Optimized Voxel for Large GNSS Network. Remote Sensing, 2020, 12, 2306.	1.8	10
52	Hybrid precipitable water vapor fusion model in China. Journal of Atmospheric and Solar-Terrestrial Physics, 2020, 208, 105387.	0.6	15
53	Preliminary result of capturing the signature of heavy rainfall events using the 2-d-/4-d water vapour information derived from GNSS measurement in Hong Kong. Advances in Space Research, 2020, 66, 1537-1550.	1.2	11
54	3â€Ð Tomographic Reconstruction of SED Plume During 17 March 2013 Storm. Journal of Geophysical Research: Space Physics, 2020, 125, e2020JA028257.	0.8	13

#	Article	IF	CITATIONS
55	Multi-Instrumental Observations of Early Morning Equatorial Plasma Depletions During the 2017 Memorial Weekend Storm. IEEE Journal of Selected Topics in Applied Earth Observations and Remote Sensing, 2020, 13, 5351-5357.	2.3	1
56	A Refinement Method of Real-Time Ionospheric Model for China. Remote Sensing, 2020, 12, 3354.	1.8	1
57	An improved ridge estimation (IRE) method for troposphere water vapor tomography. Journal of Atmospheric and Solar-Terrestrial Physics, 2020, 207, 105366.	0.6	3
58	Analysis of Ionospheric Disturbances Caused by the 2018 Bering Sea Meteor Explosion Based on GPS Observations. Sensors, 2020, 20, 3201.	2.1	9
59	A Refined Regional Model for Estimating Pressure, Temperature, and Water Vapor Pressure for Geodetic Applications in China. Remote Sensing, 2020, 12, 1713.	1.8	15
60	A Novel ENSO Monitoring Method using Precipitable Water Vapor and Temperature in Southeast China. Remote Sensing, 2020, 12, 649.	1.8	11
61	An improved GNSS tropospheric tomography method with the GPT2w model. GPS Solutions, 2020, 24, 1.	2.2	24
62	Development of Global Tropospheric Empirical Correction Model with High Temporal Resolution. Remote Sensing, 2020, 12, 721.	1.8	10
63	An Improved Rainfall Forecasting Model Based on GNSS Observations. IEEE Transactions on Geoscience and Remote Sensing, 2020, 58, 4891-4900.	2.7	68
64	Improved GPT2w (IGPT2w) model for site specific zenith tropospheric delay estimation in China. Journal of Atmospheric and Solar-Terrestrial Physics, 2020, 198, 105202.	0.6	13
65	Anomaly Variation of Vegetation and Its Influencing Factors in Mainland China During ENSO Period. IEEE Access, 2020, 8, 721-734.	2.6	14
66	An improved constrained simultaneous iterative reconstruction technique for ionospheric tomography. GPS Solutions, 2020, 24, 1.	2.2	14
67	A Drought Monitoring Method Based on Precipitable Water Vapor and Precipitation. Journal of Climate, 2020, 33, 10727-10741.	1.2	41
68	Studies of precipitable water vapour characteristics on a global scale. International Journal of Remote Sensing, 2019, 40, 72-88.	1.3	17
69	A Global Model for Estimating Tropospheric Delay and Weighted Mean Temperature Developed with Atmospheric Reanalysis Data from 1979 to 2017. Remote Sensing, 2019, 11, 1893.	1.8	50
70	An ERA5â€Based Model for Estimating Tropospheric Delay and Weighted Mean Temperature Over China With Improved Spatiotemporal Resolutions. Earth and Space Science, 2019, 6, 1926-1941.	1.1	46
71	Comparisons between the WRF data assimilation and the GNSS tomography technique in retrieving 3-D wet refractivity fields in Hong Kong. Annales Geophysicae, 2019, 37, 25-36.	0.6	4
72	Ingestion of GIM-derived TEC data for updating IRI-2016 driven by effective IG indices over the European region. Journal of Geodesy, 2019, 93, 1911-1930.	1.6	13

YINBIN YAO

#	Article	IF	CITATIONS
73	Establishment of a Real-Time Local Tropospheric Fusion Model. Remote Sensing, 2019, 11, 1321.	1.8	19
74	Reconstruction of 2D/3D ionospheric disturbances in high-latitude and arctic regions during a geomagnetic storm using GNSS carrier TEC: a case study of the 2015 great storm. Journal of Geodesy, 2019, 93, 1529-1541.	1.6	8
75	Evidence of Mid- and Low-Latitude Nighttime Ionospheric \$E\$ –\$F\$ Coupling: Coordinated Observations of Sporadic \$E\$ Layers, \$F\$ -Region Field-Aligned Irregularities, and Medium-Scale Traveling Ionospheric Disturbances. IEEE Transactions on Geoscience and Remote Sensing, 2019, 57, 7547-7557.	2.7	13
76	Geodetic and hydrological measurements reveal the recent acceleration of groundwater depletion in North China Plain. Journal of Hydrology, 2019, 575, 1065-1072.	2.3	79
77	A new datum jump detection and mitigation method of Real-Time Service (RTS) clock products. GPS Solutions, 2019, 23, 1.	2.2	5
78	A new troposphere tomography algorithm with a truncation factor model (TFM) for GNSS networks. GPS Solutions, 2019, 23, 1.	2.2	21
79	A New GPS SNR-based Combination Approach for Land Surface Snow Depth Monitoring. Scientific Reports, 2019, 9, 3814.	1.6	18
80	Multi-Time Scale Analysis of Regional Aerosol Optical Depth Changes in National-Level Urban Agglomerations in China Using Modis Collection 6.1 Datasets from 2001 to 2017. Remote Sensing, 2019, 11, 201.	1.8	18
81	Real-Time Global Ionospheric Map and Its Application in Single-Frequency Positioning. Sensors, 2019, 19, 1138.	2.1	16
82	The realization and evaluation of mixed GPS/BDS PPP ambiguity resolution. Journal of Geodesy, 2019, 93, 1283-1295.	1.6	5
83	Geodetic and model data reveal different spatio-temporal patterns of transient mass changes over Greenland from 2007 to 2017. Earth and Planetary Science Letters, 2019, 515, 154-163.	1.8	21
84	An improved pixel-based water vapor tomography model. Annales Geophysicae, 2019, 37, 89-100.	0.6	6
85	Short-term rainfall forecast model based on the improved BP–NN algorithm. Scientific Reports, 2019, 9, 19751.	1.6	50
86	A New Typhoon-Monitoring Method Using Precipitation Water Vapor. Remote Sensing, 2019, 11, 2845.	1.8	24
87	Improved Drought Monitoring Index Using GNSS-Derived Precipitable Water Vapor over the Loess Plateau Area. Sensors, 2019, 19, 5566.	2.1	16
88	Precipitable water vapor fusion: an approach based on spherical cap harmonic analysis and Helmert variance component estimation. Journal of Geodesy, 2019, 93, 2605-2620.	1.6	29
89	A new method for vertical stratification of zenith tropospheric delay. Advances in Space Research, 2019, 63, 2857-2866.	1.2	13
90	GNSS-derived PWV and comparison with radiosonde and ECMWF ERA-Interim data over mainland China. Journal of Atmospheric and Solar-Terrestrial Physics, 2019, 182, 85-92.	0.6	61

#	Article	IF	CITATIONS
91	Study on the plasmaspheric Weddell Sea Anomaly based on COSMIC onboard GPS measurements. Journal of Atmospheric and Solar-Terrestrial Physics, 2019, 192, 104923.	0.6	6
92	On the errors-in-variables model with inequality constraints of dependent variables for geodetic transformation. Survey Review, 2019, 51, 166-171.	0.7	2
93	Accuracy and reliability of tropospheric wet refractivity tomography with GPS, BDS, and GLONASS observations. Advances in Space Research, 2019, 63, 2836-2847.	1.2	14
94	Tridimensional reconstruction of the Co-Seismic Ionospheric Disturbance around the time of 2015 Nepal earthquake. Journal of Geodesy, 2018, 92, 1255-1266.	1.6	19
95	Evaluation and analysis of real-time precise orbits and clocks products from different IGS analysis centers. Advances in Space Research, 2018, 61, 2942-2954.	1.2	54
96	A new weighted mean temperature model in China. Advances in Space Research, 2018, 61, 402-412.	1.2	11
97	GPS-based PWV for precipitation forecasting and its application to a typhoon event. Journal of Atmospheric and Solar-Terrestrial Physics, 2018, 167, 124-133.	0.6	73
98	An empirical zenith wet delay correction model using piecewise height functions. Annales Geophysicae, 2018, 36, 1507-1519.	0.6	8
99	Plasmaspheric Electron Content Inferred from Residuals between GNSS-Derived and TOPEX/JASON Vertical TEC Data. Remote Sensing, 2018, 10, 621.	1.8	20
100	Geodetic measurements reveal short-term changes of glacial mass near Jakobshavn Isbræ (Greenland) from 2007 to 2017. Earth and Planetary Science Letters, 2018, 503, 216-226.	1.8	10
101	Development and Assessment of the Atmospheric Pressure Vertical Correction Model With ERAâ€Interim and Radiosonde Data. Earth and Space Science, 2018, 5, 777-789.	1.1	5
102	Establishment and Evaluation of a New Meteorological Observation-Based Grid Model for Estimating Zenith Wet Delay in Ground-Based Global Navigation Satellite System (GNSS). Remote Sensing, 2018, 10, 1718.	1.8	13
103	Extending a model for water vapor sounding by ground-based GNSS in the vertical direction. Journal of Atmospheric and Solar-Terrestrial Physics, 2018, 179, 358-366.	0.6	8
104	Mapping seasonal impervious surface dynamics in Wuhan urban agglomeration, China from 2000 to 2016. International Journal of Applied Earth Observation and Geoinformation, 2018, 70, 51-61.	1.4	26
105	Real-time precise point positioning-based zenith tropospheric delay for precipitation forecasting. Scientific Reports, 2018, 8, 7939.	1.6	39
106	GPS Interferometric Reflectometry Reveals Cyclic Elevation Changes in Thaw and Freezing Seasons in a Permafrost Area (Barrow, Alaska). Geophysical Research Letters, 2018, 45, 5581-5589.	1.5	27
107	Near-global GPS-derived PWV and its analysis in the El Niño event of 2014–2016. Journal of Atmospheric and Solar-Terrestrial Physics, 2018, 179, 69-80.	0.6	25
108	An analytical approach to evaluate point cloud registration error utilizing targets. ISPRS Journal of Photogrammetry and Remote Sensing, 2018, 143, 48-56.	4.9	7

#	Article	IF	CITATIONS
109	An Optimal Tropospheric Tomography Method Based on the Multi-GNSS Observations. Remote Sensing, 2018, 10, 234.	1.8	23
110	Influence of Three Ionospheric Models on Navigation Positioning Accuracy in China. Lecture Notes in Electrical Engineering, 2018, , 493-500.	0.3	0
111	GGOS tropospheric delay forecast product performance evaluation and its application in real-time PPP. Journal of Atmospheric and Solar-Terrestrial Physics, 2018, 175, 1-17.	0.6	19
112	A modified three-dimensional ionospheric tomography algorithm with side rays. GPS Solutions, 2018, 22, 1.	2.2	15
113	Troposphere Water Vapour Tomography: A Horizontal Parameterised Approach. Remote Sensing, 2018, 10, 1241.	1.8	11
114	An optimal tropospheric tomography approach with the support of an auxiliary area. Annales Geophysicae, 2018, 36, 1037-1046.	0.6	14
115	An Improved Iterative Algorithm for Ionospheric Tomography Reconstruction by Using the Automatic Search Technology of Relaxation Factor. Radio Science, 2018, 53, 1051-1066.	0.8	15
116	Global ionospheric modeling based on multi-GNSS, satellite altimetry, and Formosat-3/COSMIC data. GPS Solutions, 2018, 22, 1.	2.2	35
117	Analysis of Ionospheric Anomalous Disturbance During a Heavy Rainfall. Lecture Notes in Electrical Engineering, 2018, , 233-242.	0.3	0
118	A Troposphere Tomography Method by Combining the Truncation Coefficient and Variance Component Analysis. Lecture Notes in Electrical Engineering, 2018, , 3-16.	0.3	0
119	A novel, optimized approach of voxel division for water vapor tomography. Meteorology and Atmospheric Physics, 2017, 129, 57-70.	0.9	26
120	Modeling the plasmasphere based on LEO satellites onboard GPS measurements. Journal of Geophysical Research: Space Physics, 2017, 122, 1221-1233.	0.8	19
121	A clear link connecting the troposphere and ionosphere: ionospheric reponses to the 2015 Typhoon Dujuan. Journal of Geodesy, 2017, 91, 1087-1097.	1.6	28
122	Contribution of solar radiation and geomagnetic activity to global structure of 27-day variation of ionosphere. Journal of Geodesy, 2017, 91, 1299-1311.	1.6	8
123	Method for evaluating real-time GNSS satellite clock offset products. GPS Solutions, 2017, 21, 1417-1425.	2.2	36
124	A two-step ionospheric modeling algorithm considering the impact of GLONASS pseudo-range inter-channel biases. Journal of Geodesy, 2017, 91, 1435-1446.	1.6	5
125	An Accurate Height Reduction Model for Zenith Tropospheric Delay Correction Using ECMWF Data. Lecture Notes in Electrical Engineering, 2017, , 337-348.	0.3	2
126	Enhancing real-time precise point positioning with zenith troposphere delay products and the determination of corresponding tropospheric stochastic models. Geophysical Journal International, 2017, 208, 1217-1230.	1.0	17

#	Article	IF	CITATIONS
127	Global ionosphere maps based on GNSS, satellite altimetry, radio occultation and DORIS. GPS Solutions, 2017, 21, 639-650.	2.2	38
128	Establishing a method of short-term rainfall forecasting based on GNSS-derived PWV and its application. Scientific Reports, 2017, 7, 12465.	1.6	100
129	GLONASS inter-frequency phase bias rate estimation by single-epoch or Kalman filter algorithm. GPS Solutions, 2017, 21, 1871-1882.	2.2	9
130	Transient Variations in Glacial Mass Near Upernavik IsstrÃ,m (West Greenland) Detected by the Combined Use of GPS and GRACE Data. Journal of Geophysical Research: Solid Earth, 2017, 122, 10,626.	1.4	17
131	Improved method to estimate undifferenced satellite fractional cycle biases using network observations to support PPP ambiguity resolution. GPS Solutions, 2017, 21, 1369-1378.	2.2	11
132	On the coseismic ionospheric disturbances after the Nepal Mw7.8 earthquake on April 25, 2015 using GNSS observations. Advances in Space Research, 2017, 59, 103-113.	1.2	16
133	Bayesian inference for the Errors-In-Variables model. Studia Geophysica Et Geodaetica, 2017, 61, 35-52.	0.3	20
134	An improved troposphere tomographic approach considering the signals coming from the side face of the tomographic area. Annales Geophysicae, 2017, 35, 87-95.	0.6	20
135	An Improved Tomography Approach Based on Adaptive Smoothing and Ground Meteorological Observations. Remote Sensing, 2017, 9, 886.	1.8	20
136	AÂtroposphere tomography method considering the weighting of input information. Annales Geophysicae, 2017, 35, 1327-1340.	0.6	7
137	A method to improve the utilization of GNSS observation for water vapor tomography. Annales Geophysicae, 2016, 34, 143-152.	0.6	31
138	Potential Seasonal Terrestrial Water Storage Monitoring from GPS Vertical Displacements: A Case Study in the Lower Three-Rivers Headwater Region, China. Sensors, 2016, 16, 1526.	2.1	19
139	An improved global zenith tropospheric delay model GZTD2 considering diurnal variations. Nonlinear Processes in Geophysics, 2016, 23, 127-136.	0.6	45
140	Large-scale traveling ionospheric disturbances using ionospheric imaging at storm time: A case study on 17 march 2013. Journal of Atmospheric and Solar-Terrestrial Physics, 2016, 145, 12-20.	0.6	9
141	The Research on Four-Dimensional Water Vapor Tomography Based on Real-Time PPP Technique. Lecture Notes in Electrical Engineering, 2016, , 3-14.	0.3	1
142	A new computerized ionosphere tomography model using the mapping function and an application to the study of seismic-ionosphere disturbance. Journal of Geodesy, 2016, 90, 741-755.	1.6	11
143	Maximally Using GPS Observation for Water Vapor Tomography. IEEE Transactions on Geoscience and Remote Sensing, 2016, 54, 7185-7196.	2.7	38
144	Analysis of the global ionospheric disturbances of the March 2015 great storm. Journal of Geophysical Research: Space Physics, 2016, 121, 12,157.	0.8	36

#	Article	IF	CITATIONS
145	A method of undifferenced ambiguity resolution for GPS+GLONASS precise point positioning. Scientific Reports, 2016, 6, 26334.	1.6	8
146	PPP Sliding Window Algorithm and Its Application in Deformation Monitoring. Scientific Reports, 2016, 6, 26497.	1.6	7
147	A global empirical model for estimating zenith tropospheric delay. Science China Earth Sciences, 2016, 59, 118-128.	2.3	9
148	Analysis of precipitable water vapor and surface temperature variation over Qinghai-Tibetan Plateau from 1979 to 2014. Chinese Science Bulletin, 2016, 61, 1462-1477.	0.4	8
149	Tomographic reconstruction of ionospheric electron density during the storm of 5-6 August 2011 using multi-source data. Scientific Reports, 2015, 5, 13042.	1.6	11
150	On total least squares for quadratic form estimation. Studia Geophysica Et Geodaetica, 2015, 59, 366-379.	0.3	16
151	Research on global plasmaspheric electron content by using LEO occultation and GPS data. Advances in Space Research, 2015, 55, 2248-2255.	1.2	15
152	A New Ionosphere Tomography Algorithm With Two-Grid Virtual Observations Constraints and Three-Dimensional Velocity Profile. IEEE Transactions on Geoscience and Remote Sensing, 2015, 53, 2373-2383.	2.7	17
153	Modeling regional ionospheric delay with ground-based BeiDou and GPS observations in China. GPS Solutions, 2015, 19, 649-658.	2.2	32
154	ITG: A New Clobal GNSS Tropospheric Correction Model. Scientific Reports, 2015, 5, 10273.	1.6	52
155	On partial errors-in-variables models with inequality constraints of parameters and variables. Journal of Geodesy, 2015, 89, 111-119.	1.6	27
156	A global empirical model for mapping zenith wet delays onto precipitable water vapor using GGOS Atmosphere data. Science China Earth Sciences, 2015, 58, 1361-1369.	2.3	9
157	Temporal and Spatial Ionospheric Variations of 20 April 2013 Earthquake in Yaan, China. IEEE Geoscience and Remote Sensing Letters, 2015, 12, 2242-2246.	1.4	15
158	GTm-III: a new global empirical model for mapping zenith wet delays onto precipitable water vapour. Geophysical Journal International, 2014, 197, 202-212.	1.0	57
159	A New Method to Accelerate PPP Convergence Time by using a Global Zenith Troposphere Delay Estimate Model. Journal of Navigation, 2014, 67, 899-910.	1.0	22
160	Improved one/multi-parameter models that consider seasonal and geographic variations for estimating weighted mean temperature in ground-based GPS meteorology. Journal of Geodesy, 2014, 88, 273-282.	1.6	60
161	An Improved Iterative Algorithm for 3-D Ionospheric Tomography Reconstruction. IEEE Transactions on Geoscience and Remote Sensing, 2014, 52, 4696-4706.	2.7	40
162	Study of the 2013 Lushan M7.0 earthquake coseismic ionospheric disturbances. Advances in Space Research, 2014, 54, 2194-2199.	1.2	4

#	Article	IF	CITATIONS
163	Analysis of the global T m–T s correlation and establishment of the latitude-related linear model. Science Bulletin, 2014, 59, 2340-2347.	1.7	36
164	Impact of GLONASS pseudorange inter-channel biases on satellite clock corrections. GPS Solutions, 2014, 18, 323-333.	2.2	16
165	A new ionospheric tomography model combining pixel-based and function-based models. Advances in Space Research, 2013, 52, 614-621.	1.2	24
166	GLONASS pseudorange inter-channel biases and their effects on combined GPS/GLONASS precise point positioning. GPS Solutions, 2013, 17, 439-451.	2.2	87
167	A new LS+AR model with additional error correction for polar motion forecast. Science China Earth Sciences, 2013, 56, 818-828.	2.3	11
168	An improved approach to model regional ionosphere and accelerate convergence for precise point positioning. Advances in Space Research, 2013, 52, 1406-1415.	1.2	18
169	Application of hybrid regularization method for tomographic reconstruction of midlatitude ionospheric electron density. Advances in Space Research, 2013, 52, 2215-2225.	1.2	25
170	Clobal empirical model for mapping zenith wet delays onto precipitable water. Journal of Geodesy, 2013, 87, 439-448.	1.6	47
171	Temporal and spatial variations in ionospheric electron density profiles over South Africa during strong magnetic storms. Natural Hazards and Earth System Sciences, 2013, 13, 375-384.	1.5	8
172	GWMT Global Atmospheric Weighted Mean Temperature Models: Development and Refinement. Lecture Notes in Electrical Engineering, 2013, , 487-500.	0.3	4
173	Research on Receiver Clock Jump Detection and Processing in Precise Point Positioning. Lecture Notes in Electrical Engineering, 2013, , 145-151.	0.3	0
174	A globally applicable, season-specific model for estimating the weighted mean temperature of the atmosphere. Journal of Geodesy, 2012, 86, 1125-1135.	1.6	94
175	Clinical investigation on application of water swallowing to MR esophagography. European Journal of Radiology, 2012, 81, 1980-1985.	1.2	8
176	Analysis of pre-earthquake ionospheric anomalies before the global <i>M</i> = 7.0+ earthquakes in 2010. Natural Hazards and Earth System Sciences, 2012, 12, 575-585.	1.5	52
177	Analysis of ionospheric anomalies before the 2011 M w 9.0 Japan earthquake. Science Bulletin, 2012, 57, 500-510.	1.7	55
178	Research and realization of seamless splicing of quasi-geoid. Geo-Spatial Information Science, 2010, 13, 56-59.	2.4	0
179	Theory and realization of GPS orbit integration. Geo-Spatial Information Science, 2008, 11, 1-5.	2.4	1

 $\hfill Research on the estimation method for Earth rotation parameters. , 2008, , .$

#	Article	IF	CITATIONS
181	On the non-linear motion of IGS station. Geo-Spatial Information Science, 2007, 10, 240-244.	2.4	2
182	Earth rotation parameter estimation by GPS observations. Geo-Spatial Information Science, 2006, 9, 260-264.	2.4	2
183	Crustal movement patterns of china continent measured by GPS. Geo-Spatial Information Science, 2003, 6, 57-60.	2.4	1
184	Multi-quadric equations interpolation and its applications to the establishment of crustal movement speed field. Geo-Spatial Information Science, 2002, 5, 1-5.	2.4	3
185	Theoretic research on robustified least squares estimator based on equivalent variance-covariance. Geo-Spatial Information Science, 2001, 4, 1-8.	2.4	1